Journal of Photopolymer Science and Technology
Volume 31, Number 2 (2018) 249–255 ©2018SPST

Dual-tone Application of a Tin-Oxo Cage Photoresist Under E-beam and EUV Exposure

Yu Zhang[1], Jarich Haitjema[1], Milos Baljozovic[2], Michaela Vockenhuber[2], Dimitrios Kazazis[2], Thomas A. Jung[2], Yasin Ekinci[2], and Albert M. Brouwer[1,3*]

[1] *Advanced Research Center for Nanolithography, P.O. Box 93019, 1090 BA Amsterdam, The Netherlands*
[2] *Paul Scherrer Institut, 5232 Villigen, Switzerland*
[3] *van't Hoff Institute for Molecular Sciences, Faculty of Science, University of Amsterdam, P.O. Box 94157, 1090 GD Amsterdam, The Netherlands*
**f.brouwer@arcnl.nl*

We report on the dual-tone property of the tin-oxo cage $(BuSn)_{12}O_{14}(OH)_6](OH)_2$ photoresist. After exposing the resist film to a low dose extreme ultraviolet radiation or electron beam, applying a post exposure bake step and development with isopropanol/H_2O (2:1), a positive tone image is observed. The previously observed negative tone is found at higher doses. Atomic force microscopy and scanning electron microscopy were used to characterize the topography of the patterns. X-ray photoelectron spectroscopy was used to elucidate the chemical changes of the tin-oxo cages under different conditions. The photoresist, which has dual-tone property, paves the way to fabricate sophisticated structures in a single photoresist layer or may lead to metal-containing resists with improved sensitivity.
Keywords: Dual-tone photoresist, EUV photoresist, Inorganic photoresist, Tin-oxo cages, Tone conversion, Mechanism

1. Introduction

Photoresist performance plays a key role in high-resolution photolithography and must be adapted to the continuously decreased wavelength of the light source in lithography tools. Chemically-amplified photoresists are widely used in ultraviolet (UV) and deep UV (DUV) lithography [1,2]. With the increasing requirements on photoresist performance, such as resolution, sensitivity and line edge roughness, inorganic molecular photoresists, especially metal containing photoresists, have attracted attention due to their small molecular size, strong etching resistance and high absorption cross-section at the extreme ultraviolet (EUV) wavelength of 13.5 nm [3-7].

Tin-oxo cages are known to work as negative tone photoresists under EUV and DUV exposure and in electron beam lithography. They are highly sensitive and potentially give high resolution due to their high EUV absorption cross-section and small molecular size [4,8-10]. To realize a negative tone pattern, a 30 mJ/cm^2 EUV dose, a post exposure bake (PEB) step (~100 °C for 2 min) and a development step (2:1 IPA/H_2O for 30 s) are needed [4,8].

Dual-tone properties of photoresists have been reported in recent years [11-16]. Switching between positive and negative tone patterns is usually achieved by changing the developer [3,11,13]. In the present work, a dual-tone patterning is realized by performing the PEB step at an elevated temperature (150 °C for 2 min) after EUV or e-beam exposure and before development (2:1 IPA/H_2O for 30 s). At low doses a positive tone is achieved, while higher doses result in a negative tone pattern. The dual-tone property of the tin-oxo cage photoresist gives the possibility to fabricate positive and negative tone structures in a single step.

2. Experimental

2.1. Materials

The tin-oxo cages with hydroxide as counterion $[(BuSn)_{12}O_{14}(OH)_6](OH)_2$ abbreviated here as TinOH was synthesized according to the literature [8,17]. The compound was dissolved in toluene (~10 mg/mL for patterning and 2 mg/mL for XPS) and the solution was filtered through an 0.2 μm PTFE filter before spin coating. The solutions were

Received April 21, 2018
Accepted May 17, 2018

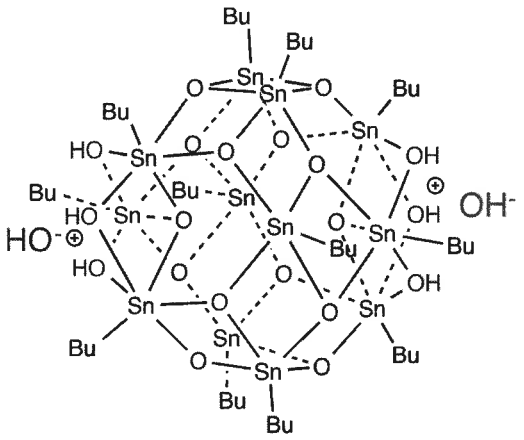

Fig. 1. The chemical structure of the tin-oxo cage with hydroxides as counterions (TinOH).

spin coated (700 rpm/s acceleration, 2500 rpm for 35 s) on different substrates (pre-cleaned and HDMS-treated Si for patterning, 20 nm Au coated glass for XPS) to give 20 ± 2 nm thin films for patterning and 5 ± 2 nm thin films for XPS. Post application bake (PAB) (90 °C, 1 min) was applied to remove residual solvent. After exposure, the samples were baked at 150 °C for 2 min, developed in a 2:1 isopropanol/H_2O mixture for 30 s, rinsed with water for 30 s, blown dry with N_2, and finally baked (hard bake; HAB) at 150 °C for 1 min to further remove residual solvent.

2.2. Exposure

E-beam lithography was performed using a Raith e-line lithography system (30 keV, 32 pA). EUV (13.5 nm, 92 eV) interference lithography was performed at the XIL-II beamline of the Swiss Light Source, the synchrotron light source at the Paul Scherrer Institute (PSI).

2.3. Characterization

Atomic force microscopy (AFM, Bruker Dimension Icon) was used to check the film thickness and the topography of the exposed pattern. Scanning electron microscopy (SEM) images were recorded using the FEI Verios 460. X-ray photoelectron spectroscopy (XPS) using a SPECS analyzer Phoibos 150, with a monochromatic AlK_α source (1486.6 eV, power 200 W) was used to characterize the chemical changes of the resist thin film under different conditions. Thermal gravimetric analysis (TGA) was performed with a NETZSCH STA 449 F3 Jupiter equipped with automatic sample changer.

3. Results and discussion

3.1. Topography characterization

The tin-oxo cage with hydroxide counterions (TinOH, see Fig. 1) was used as a model photoresist. The photoresist solution was spin-coated on Si wafers and exposed to EUV or e-beam.

E-beam lithography was used to write 1 µm line/space patterns on the tin-oxo cage layer. After exposing the thin layer to different e-beam doses and applying PEB, development, rinse and HAB, the topography of the patterns was studied using AFM. Different tone patterns were observed on the same sample, as depicted in Fig. 2. The exposed part was removed in the first pattern in Fig. 2a, giving the positive tone pattern at a dose of 50 µC/cm^2. With 100 µC/cm^2 (Fig. 2b), the exposed part was partly removed, making it difficult to distinguish the

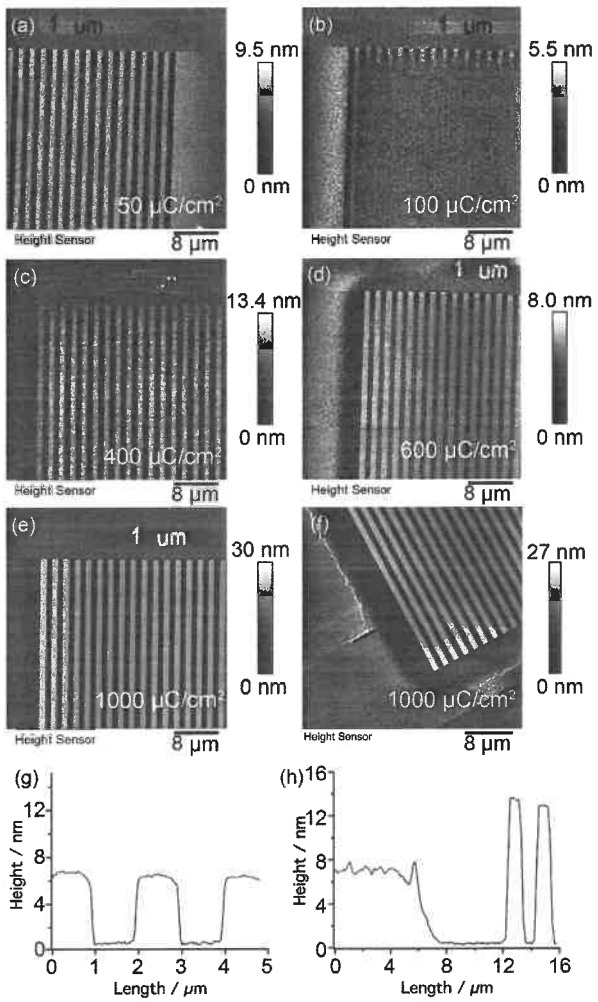

Fig. 2. AFM images of tin-oxo cage photoresist patterned using e-beam lithography performed with different doses, a) 50 µC/cm^2, b) 100 µC/cm^2, c) 400 µC/cm^2, d) 600 µC/cm^2, e) 1000 µC/cm^2, f) 1000 µC/cm^2, g) cross section of positive tone pattern in a; h) cross section of negative tone pattern in f.

exposed and unexposed areas. When the dose was increased to 400 μC/cm^2 (Fig. 2c) and 600 μC/cm^2 (Fig. 2d), the negative tone pattern started to grow. At 1000 μC/cm^2 (Figs. 2e and 2f), the exposed part is clearly negative tone. The edge of the high dose exposed part, however, was removed by the developer, and it thus shows a positive tone behavior. The spaces between the exposed lines were totally cleared. The phenomenon can be explained as a result of the proximity effect in e-beam lithography [18]. The high-energy primary electrons can interact with the resist layer or further below at the interface of the resist and the substrate where low-energy electrons are generated that diffuse to the unexposed areas. For this reason, the edge of the high dose exposed pattern behaves like the low dose exposed material, and gives rise to a positive tone. The higher the dose, the stronger the proximity effect will be. When the sample was exposed to 400 μC/cm^2 and 600 μC/cm^2 dose, respectively, the low energy electrons generated by the proximity effect are insufficient to convert the edge part. With a higher dose of 1000 μC/cm^2, the proximity effect is quite strong. Not only were the spaces between the exposed lines cleared, but also the area at the edge of the pattern was cleared. The different tones in the different images are clearly seen in the "1 um" marker at the top of each image.

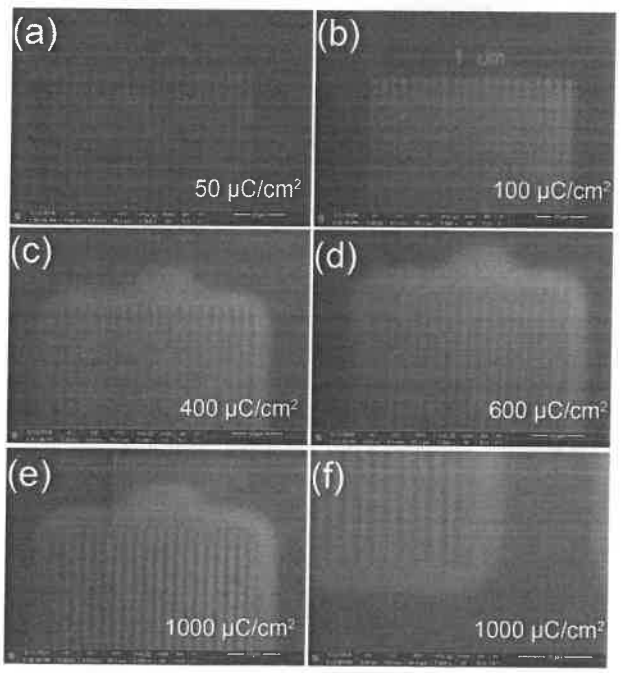

Fig. 3. SEM images of tin-oxo cage photoresist TinOH patterned using e-beam lithography with different doses, a) 50 μC/cm^2, b) 100 μC/cm^2, c) 400 μC/cm^2, d) 600 μC/cm^2, e) 1000 μC/cm^2, f) 1000 μC/cm^2, followed by PEB at 150°C for 2 min, development with 2:1 IPA/H_2O for 30 s, rinse with water for 10 s and HAB.

Cross sections of the patterns in Figs. 2a and 2f are displayed in Figs. 2g and 2h. The original film thickness was 20 ± 2 nm. As we can observe from Fig. 2e, after all the processing the unexposed part left a ~7 nm thick film, and the 50 μC/cm^2 exposed part was totally removed. In Fig. 2f, the film thickness of the 1000 μC/cm^2 exposed part is 14 nm. The space between the exposed parts and the edge part of the pattern was cleaned. The area far away from the positive tone edge part of the pattern still exhibits a 7 nm thick film after the completed process. The width of the positive tone edge of the pattern (around 4.5 μm) could correspond to the diffusion length of the electrons generated from the proximity effect at the interface below the resist layer [19].

SEM was also used to characterize the same e-beam exposed pattern. Since we observed (Fig. 2a) that the exposed part responds with a positive tone, the bright lines in Fig. 3a represent the positive tone pattern. With the dose increasing from 50 to 1000 μC/cm^2, the negative tone pattern starts and the edge effect also becomes obvious. The signal intensity cannot be used to distinguish the tone properties in these SEM images. AFM is a more appropriate technique to characterize the tone property.

The dual-tone phenomenon was also observed when the tin-oxo cage film was exposed to EUV. AFM and SEM were used to characterize the patterns from the EUV exposure. With the dose increasing from 3.6 to 53.5 mJ/cm^2, the positive tone first starts to show and then converts to negative tone pattern as shown in Figs. 4a to f.

We present the edges of the patterns from two exposure doses (3.6 mJ/cm^2, 53.5 mJ/cm^2) in Fig. 5. The SEM images of a 3.6 mJ/cm^2 EUV exposed 100 nm pitch pattern is displayed in Fig. 5a, the AFM image is in Fig. 5b, and a cross section of Fig. 5b is displayed in Fig. 5c.

A clear positive tone pattern is observed in Fig. 5b. The depth of the positive tone pattern is around 7 nm, similarly to the result observed from the e-beam exposure. The remaining film thickness is also around 7 nm. Towards the edge of the pattern, the depth of the exposed line becomes lower because of the even lower dose of EUV at the edge part. The SEM and AFM results for a dose of 53.5 mJ/cm^2 are presented in Figs. 5d, e and f. At this exposure the negative tone pattern starts to grow, while positive tone response was observed at the edge part of the pattern. The dose at the edge part is high enough to generate a positive tone, but the interference line cannot be observed any more. The remaining thickness of the unexposed area is around 6 nm. Above all, the dual-tone property of the TinOH can

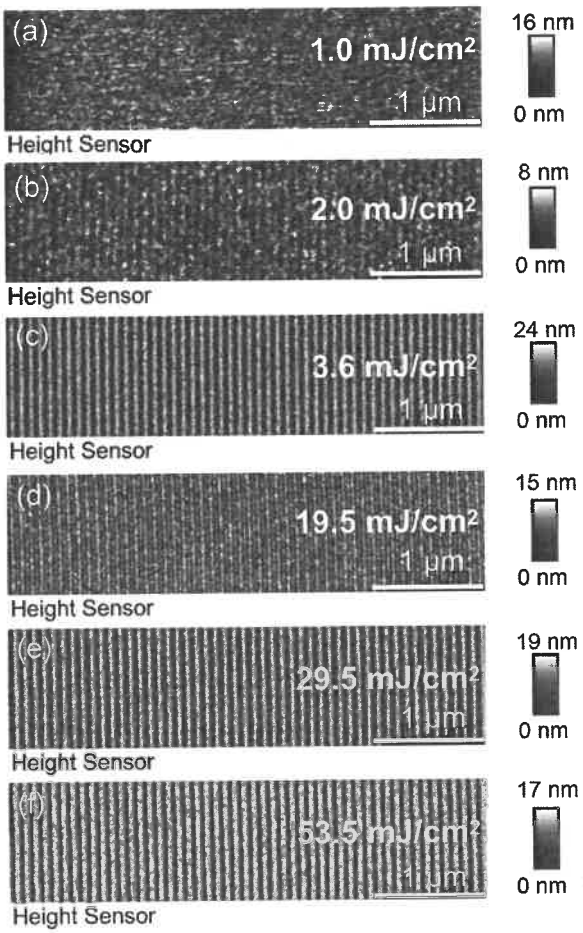

Fig. 4. AFM images of tin-oxo cage photoresist patterned by EUV lithography (100 nm pitch) performed with different doses, a) 1 mJ/cm^2, b) 2 mJ/cm^2, c) 3.6 mJ/cm^2, d) 19.5 mJ/cm^2, e) 29.5 mJ/cm^2, f) 53.5 mJ/cm^2.

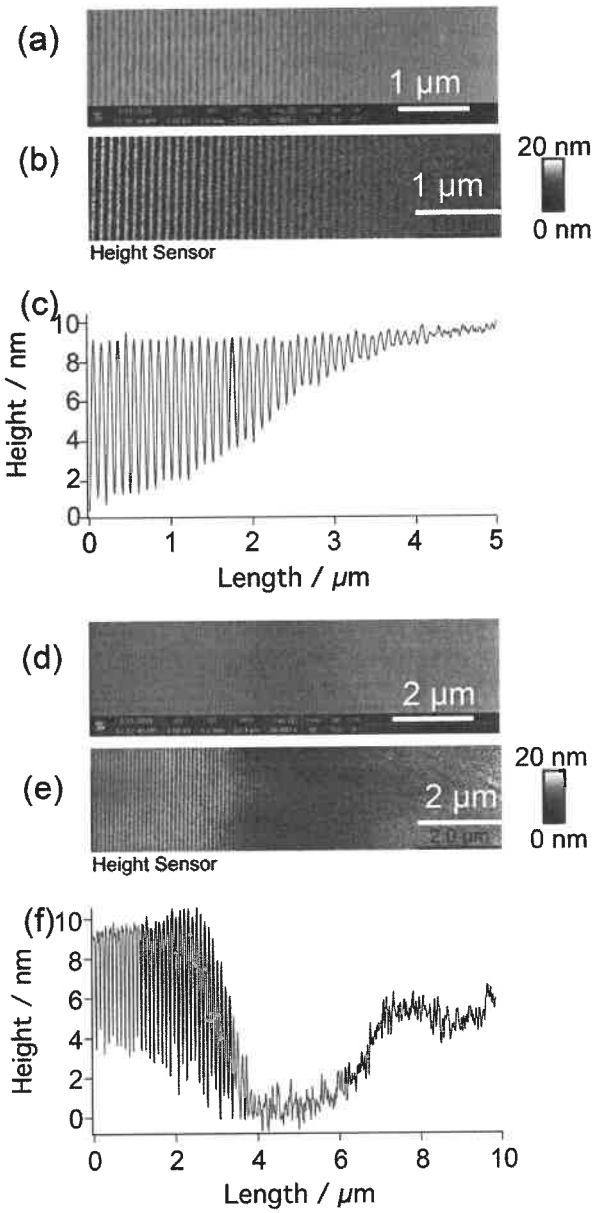

Fig. 5. a) SEM images of 3.6 mJ/cm^2 EUV dose patterned tin-oxo cage thin film, b) AFM images of 3.6 mJ/cm^2 EUV dose patterned tin-oxo cage thin film, c) cross section of image in b; d) SEM images of 53.5 mJ/cm^2 EUV dose patterned tin-oxo cage thin film, e) AFM images of 53.5 mJ/cm^2 EUV dose patterned tin-oxo cage thin film, f) cross section of image in e.

be observed for both EUV and e-beam exposure.

The curves of remaining film thickness of TinOH as a function of EUV and e-beam dose are shown in Fig. 6. After performing PEB at 150 °C for 2 min and development (2:1 IPA/H_2O for 30 s), the unexposed part has ~40% film thickness remaining. For the e-beam exposed sample, when the film was exposed to 50 - 200 μC/cm^2 the film was totally cleaned. From 500 to 1300 μC/cm^2, there is a flat zone. With dose increasing from 1300 to 2000 μC/cm^2, the remaining film thickness increased. When the dose was increased above 2000 μC/cm^2, the film thickness decreased again due to the loss of more and more of the butyl groups, leading to densification of the material. For the EUV exposed sample, the change of the film thickness shows a similar tendency. At the first stage (dose below 2 mJ/cm^2), the film thickness decreased with increase of the dose. As the dose was further increased, the remaining film thickness increased after overcoming a flat zone (dose 3 to 6 mJ/cm^2). The negative tone reaches a maximum when the dose reaches to 10 mJ/cm^2. The film thickness decreased slightly when higher dose was applied due to the densification of the material, similarly to the e-beam result. The plots of film thickness vs. dose again illustrate the dual-tone property of TinOH.

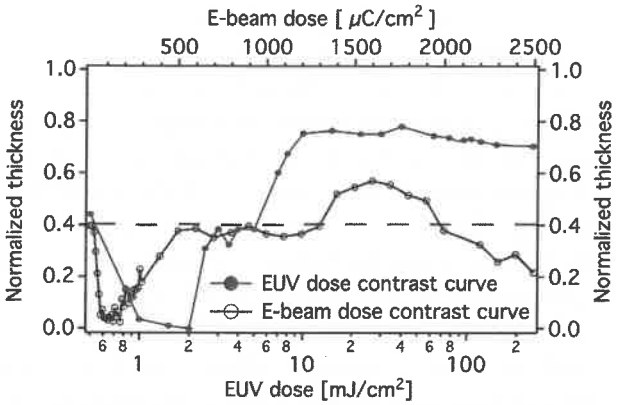

Fig. 6. Remaining layer thickness of TinOH films after EUV or e-beam exposure with post exposure bake (150 °C for 2 min) and development in 2:1 IPA/H_2O for 30 s. Dashed line represents the thickness of remaining unexposed part. The initial layer thickness was ~20 nm.

3.2. XPS characterization

The phenomenon of the dual-tone pattern has been described above. The mechanism behind this phenomenon, however, is unknown. XPS was used in an attempt to characterize chemical changes in the EUV exposed tin-oxo cage thin films, and TGA was used to investigate the thermal stability of the material.

Several samples (Table 1) were produced with different exposure and baking conditions on Au coated glass substrates for XPS analysis. The overview spectra of the samples are shown in Fig. 7. All the relevant elements present in the composition of the material are observed in the spectra as Sn 3d 3/2 and Sn 3d 5/2, C1s, and O1s peaks.

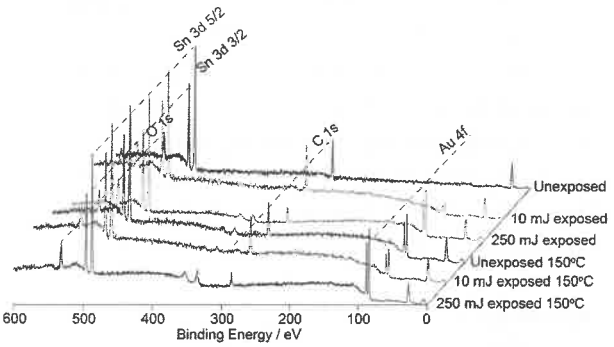

Fig. 7. Overview spectra of unexposed, 10 mJ/cm², and 250 mJ/cm² exposed TinOH thin layer sample, and another set of samples that were prepared in the same way but were subjected to post exposure bake at 150 °C for 2 min.

Additionally, in some cases Au 4f peaks are visible, originating from the gold substrate below the thin photoresist layers. Since the area of each element's peaks is related to the atomic concentration of the element in the thin film, the relative atomic composition of the samples could be calculated, and the results are listed in Table 1.

Table 1. Normalized relative atomic concentration of elements present in different tin-oxo cage samples calculated from spectra shown in Fig. 7.

Atomic.	Sn	O	C
Theoretical	12	22	48
unexposed	12	22±1	48±2
150 °C	12	18±1	50±2
10 mJ/cm²	12	22±1	50±2
10 mJ/cm²&150 °C	12	22±1	48±2
250 mJ/cm²	12	22±1	33±2
250 mJ/cm²&150 °C	12	24±1	34±2

In Table 1, all the elemental ratios are normalized to Sn. The elemental ratio of the unexposed sample agrees well with the theoretical ratio calculated from the molecular structure of the material. If there is no PEB at 150 °C the unexposed layer can be removed by the 2:1 IPA/H_2O developer [8]. When the unexposed thin film was baked at 150 °C for 2 min, a small loss of oxygen was observed. For the 10 mJ/cm² EUV exposed samples, the element ratio stayed the same as in the original film irrespective of whether the baking step was performed. For the 250 mJ/cm² EUV exposed thin films, a substantial fraction of carbon was lost while the oxygen content gained possibly by oxidation after baking at 150 °C. The loss of carbon is caused by the breaking of Sn-C bonds upon photoactivation [20]. As observed before, the film becomes insoluble in the developer at this stage of exposure and forms a negative tone pattern. PEB is not even needed although it helps to increase the sensitivity [8].

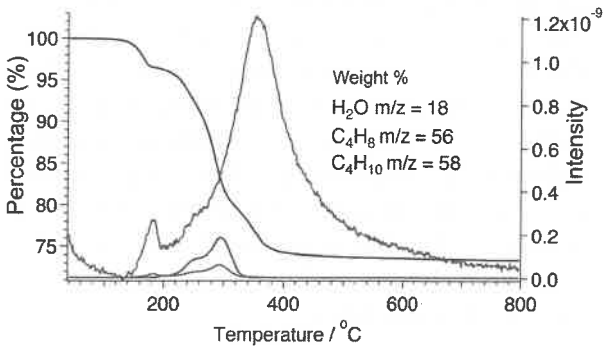

Fig. 8. TGA analysis of the TinOH powder. Weight vs. temperature (increase ca. 60 °C/min) (black), mass spectral traces corresponding to loss of water, butene and butane (green, blue and red).

A thermal gravimetric analysis (TGA) was performed on the original tin-oxo cage material in the powder form. Mass spectrometry was used to characterize the fragments lost during progressive heating. As shown in Fig. 8, there is no obvious mass loss below 130 °C. A loss of H_2O was observed between 130 and 200 °C. The theoretical decrease in mass for loss of two H_2O molecules would be 1.5%. In Fig. 8, the mass loss at 150 °C is 1%, indicating the materials could lose more than one H_2O molecule per molecule / unit $[(BuSn)_{12}O_{14}(OH)_6](OH)_2$, which is enough to lead to the solubility change. This result also corresponds well with the O loss observed in the XPS data of the unexposed sample after baking at 150 °C. Both these results indicate that the tin cage with the hydroxide counterion may be inherently unstable. In molecular quantum chemistry calculations we observed that the OH^- ion can easily attack the tin cage as a nucleophile, and it can also act as a base and deprotonate a bridging OH group [21]. Hydrogen bonding by a few water molecules can "tame" the reactive OH^- ion. We hypothesize that loss of such solvent-water molecules and the further loss of water due to deprotonation destabilize the cage structure, making it prone to undergo ring opening and condensation reactions with neighboring cages. We also observed loss of butene and butane in the TGA experiment, but this requires temperatures > 200 °C. The results of our multi-technique analysis provide a tentative explanation for the reduced solubility of the unexposed materials after a PEB step at 150 °C for 2 min. Low dose irradiation with EUV photons or electrons probably also leads to Sn-C bond cleavage, but the chemical conversions are probably too small to be detectable in our XPS analysis. The small conversion, however, is sufficient to change the properties of the film. This makes it less sensitive to PEB, allowing the positive tone development. PMMA shows a similar tone switch in e-beam exposure, which is readily understood as a result of initial chain shortening (increasing solubility) followed by cross-linking (decreasing solubility) [16]. In our material, the explanation is still unknown. The molecular-level details of this conversion process remain to be investigated in more depth in the future.

4. Conclusion

Dual-tone patterns can be realized by using tin-oxo cages as a photoresist for EUV and e-beam exposures. Upon baking the unexposed TinOH film at ~150 °C, the solubility decreased. Considering the TGA results, we relate this to the water loss occurring at this temperature. In low-dose exposed regions of the same sample, however, the exposed part can still be dissolved after baking. Thus, the exposure changes the sensitivity of the material to heating. The chemical changes, which are decisive for this transition, are below or close to the limit of detection of our XPS analysis of a few percent. This indicates that the chemical modification of only a small number of the many atoms contained in the tin-oxo cages can already modify the development behavior of this resist material. Upon application of high doses of photons or electrons, in contrast, a substantial loss of carbon occurs, readily detectable by means of XPS, and the exposed part cannot be dissolved in the same developer any longer. The unexposed part can still be dissolved, provided that the baking temperature is not too high. In this way, the same film can be used to generate a positive or negative tone photoresist with the same developer.

Acknowledgements

Part of this work has been carried out at the Advanced Research Center for Nanolithography (ARCNL), a public-private partnership of University of Amsterdam (UvA), the VU university Amsterdam (VU), the Netherlands Organization for Scientific Research (NWO) and the semiconductor equipment manufacturer ASML. We thank Lianjia Wu (ARCNL) for performing the TGA measurement. M.B. and T.A.J. acknowledge the Swiss National Science Foundation (Grant no. 200020–153549, 200020-175800 and 206021-113149). This project has received funding from the EU-H2020 research and innovation program under grant agreement No. 269 having benefitted from the access provided by PSI in Villigen within the framework of the Nanoscience Foundries and Fine Analysis Europe Transnational Access Activity.

References

1. S. Matsumaru, T. Fujii, T. Kamizono, K. Suzuki, H. Yamazaki, M. Arai, Y. Komuro, A. Kawaue, D. Kawana, T. Hirayama, and K. Ohmori, *Proc. SPIE,* **9425** (2015) 94250U.
2. T. Fujii, S. Matsumaru, T. Yamada, Y. Komuro, D. Kawana, and K. Ohmori, *Proc. SPIE,* **9776** (2016) 97760Y.
3. L. Li, S. Chakrabarty, J. Jiang, B. Zhang, C. Ober, and E. P. Giannelis, *Nanoscale,* **8** (2016) 1338.
4. B. Cardineau, R. Del Re, M. Marnell, H. Al-Mashat, M. Vockenhuber, Y. Ekinci, C. Sarma, D.

A. Freedman, and R. L. Brainard, *Microelectron. Eng.*, **127** (2014) 44.
5. R. Del Re, J. Passarelli, M. Sortland, B. Cardineau, Y. Ekinci, E. Buitrago, M. Neisser, D. A. Freedman, and R. L. Brainard, *J. Micro/Nanolith. MEMS MOEMS,* **14** (2015) 043506.
6. L. Li, S. Chakrabarty, K. Spyrou, C. K. Ober, and E. P. Giannelis, *Chem. Mater.,* **27** (2015) 5027.
7. L. Li, X. Liu, S. Pal, S. Wang, C. K. Ober, and E. P. Giannelis, *Chem. Soc. Rev.*, **46** (2017) 4855.
8. J. Haitjema, Y. Zhang, M. Vockenhuber, D. Kazazis, Y. Ekinci, and A. M. Brouwer, *J. Micro/Nanolith. MEMS MOEMS,* **16** (2017) 7.
9. Y. Zhang, J. Haitjema, X. Liu, F. Johansson, A. Lindblad, S. Castellanos, N. Ottosson, and A. M. Brouwer, *J. Micro/Nanolith. MEMS MOEMS,* **16** (2017) 023510.
10. R. Fallica, J. Haitjema, L. Wu, S. Castellanos, F. Brouwer, and Y. Ekinci, *Proc. SPIE,* **10143** (2017) 101430A.
11. X. Hu, J. A. Lawrence, J. Mullahoo, Z. C. Smith, D. J. Wilson, C. R. Mace, and S. W. Thomas, *Macromolecules*, **50** (2017) 7258.
12. V. Canalejas-Tejero, S. Carrasco, F. Navarro-Villoslada, J. L. García Fierro, M. d. C. Capel-Sánchez, M. C. Moreno-Bondi, and C. A. Barrios, *J. Mater. Chem. C*, **1** (2013) 1392.
13. A. Wolfberger, A. Petritz, A. Fian, J. Herka, V. Schmidt, B. Stadlober, R. Kargl, S. Spirk, and T. Griesser, *Cellulose*, **22** (2015) 717.
14. C. Xue, D. Y. Wong, and A. M. Kasko, *Adv. Mater.*, **26** (2014) 1577.
15. J. T. A. Stephen, T. Meyers, J. B. Edson, K. Jiang, D. A. Keszler, M. K. Kocsis, A. J. Telecky, and B. J. Cardineau, *US 2016/0116839 A1* (2015) 40.
16. A. C. F. Hoole, M. E. Welland, and A. N. Broers, *Semicond. Sci. Technol.* **12** (1997) 1166.
17. C. Eychenne-Baron, F. Ribot, and C. Sanchez, *J. Org. Chem.,* **567** (1998) 137.
18. T. H. P. Chang, *J. Vac. Sci. Technol.,* **12** (1975) 1271.
19. C. A. Mack, *Proc. SPIE,* **4409** (2001) 194.
20. J. Haitjema, Y. Zhang, N. Ottosson, and A. M. Brouwer, *J. Photopolym. Sci. Technol.,* **30** (2017) 99.
21. A. M. Brouwer, unpublished results.